Heterogenous $Ni(OH)_2/NiOOH$ Redox Mediator on Bismuth Vanadate for Photoelectrochemical Oxidation of 5-Hydroxymethylfurfural

Yuming Zhang [*a] **and Klaus Hellgardt** [*a]

[a] *Department of Chemical Engineering, Imperial College London, London, SW7 2AZ, U.K*

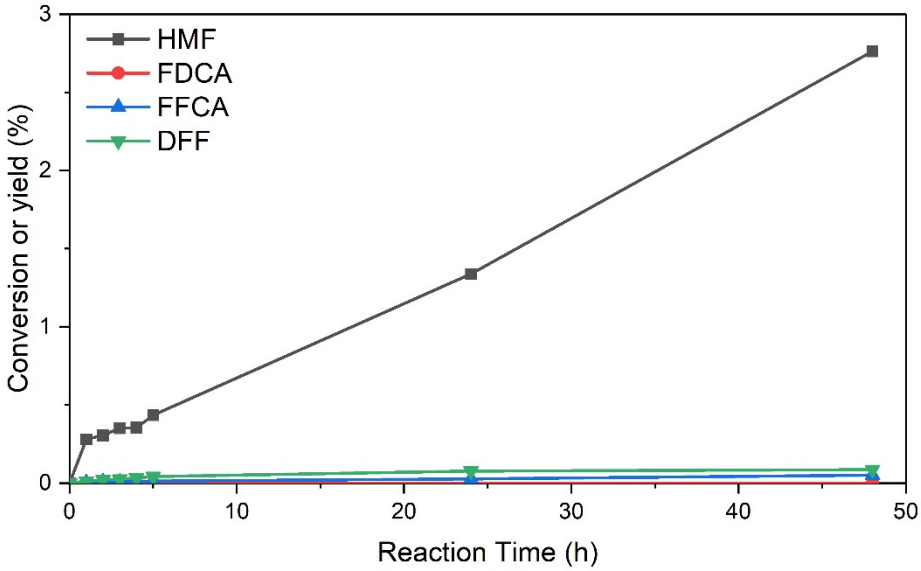

Figure S1. Product analyses following a 48-hour PEC oxidation of 5 mM HMF using a pristine $BiVO_4$ photoanode without the addition of TEMPO redox mediator.

HMF conversion remained below 3% after 48 hours of PEC operation at constant applied potential of 1.05 V *vs.* RHE, with only trace amount of DFF (0.087%) and FFCA (0.051%) formation being detected. The UV absorbance peaks obtained from HPLC were of such small magnitude that they were scarcely distinguishable from the baseline, making peak deconvolution subject to considerable uncertainties. Nonetheless, the negligible formation of desired oxidation products in the absence of redox mediators was confirmed. Although HMF remained largely unreacted, the small degree of conversion can be attributed to non-reactive adsorption of HMF molecules on the nanoporous $BiVO_4$ surface or the uncontrolled formation of side products such as humins and maleic acid. [1–3]

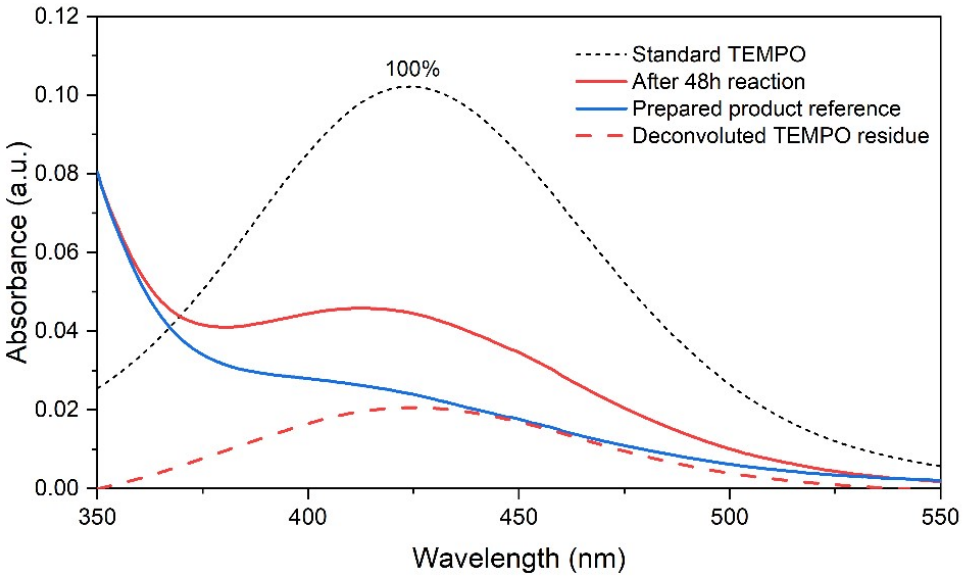

Figure S2. Normalisation of the post-reaction UV-vis spectrum for TEMPO quantification.

The red solid line shows the spectrum of an aliquot collected after a 48-hour TEMPO-assisted PEC reaction, containing oxidation products (DFF, FFCA and FDCA), residual TEMP, and some uncreated HMF. TEMPO content was quantified by subtracting a reference spectrum prepared using a solution with the same product composition, as determined by HPLC. A standard TEMPO spectrum (7.5 mM) is included as a dotted line for comparison.

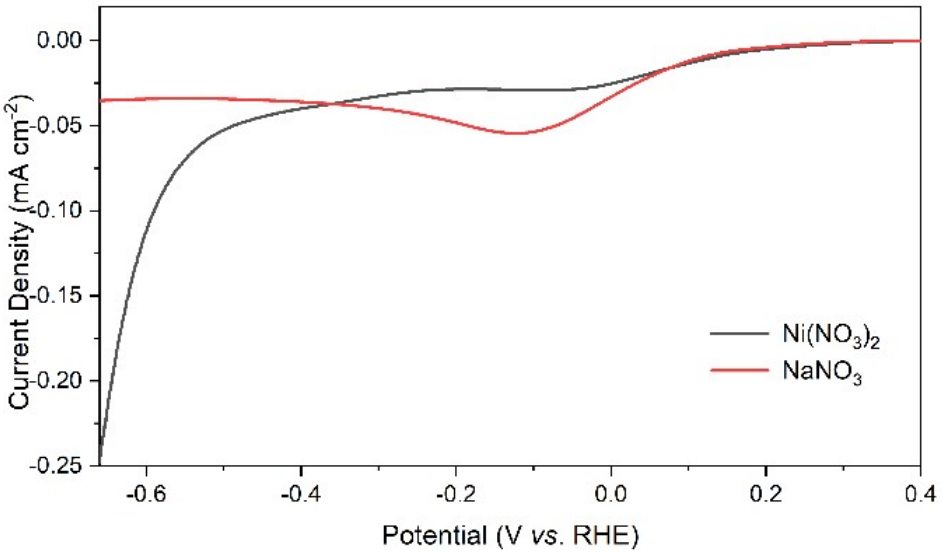

Figure S3. LSV analysis of the electroplating solution containing 10 mM $Ni(NO_3)_2$ and 20 mM $NaNO_3$ using a FTO glass working electrode. Scan rate = 10 mV s^{-1} in the cathodic (negative) direction.

Cathodic current onsets were observed at approximately 0.1 V *vs.* RHE in both solutions, which is attributed to the reduction of NO_3^-. When the solution did not contain Ni^{2+}, the current reached its maximum at -0.1 V *vs*. RHE and receded modestly as the potential was swept to the negative direction. Distinctly, the current exhibited a steep rise at -0.45 V *vs*. RHE in the $Ni(NO_3)_2$ solution. Such prominent current spike typified the reduction of Ni^{2+} to elemental $Ni_{(s)}$ (Eqn. S1).

$$Ni^{2+} + 2e^- \rightarrow Ni\downarrow \quad E^\circ = -0.26\ V \#(S1)$$

A decline in NO^{3-} reduction current was also observed in the presence of Ni^{2+}. This is due to the concurrent formation of $Ni(OH)_2$ on the electrode surface, which partially blocks the active area of the working electrode. In contrast, Na^+ is a more inert cation within the tested potential range and has a higher mobility which supports the ionic conductivity.

(a)

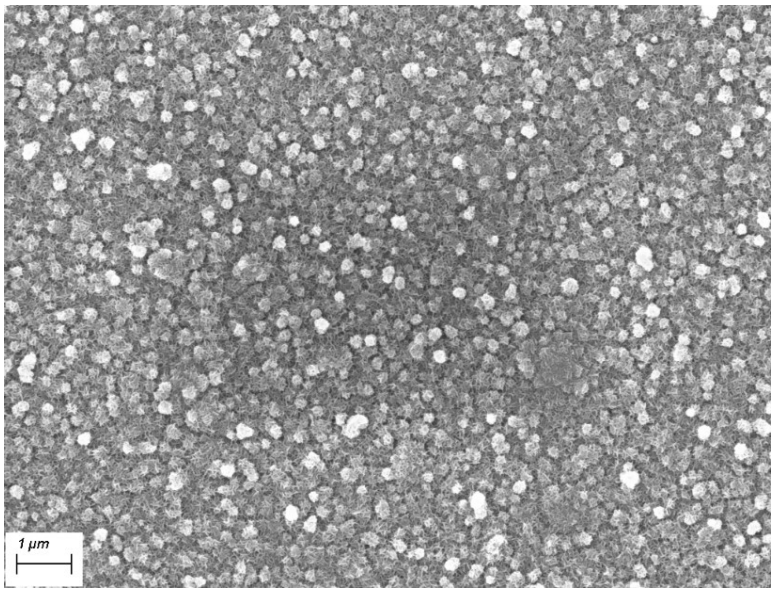

(b)

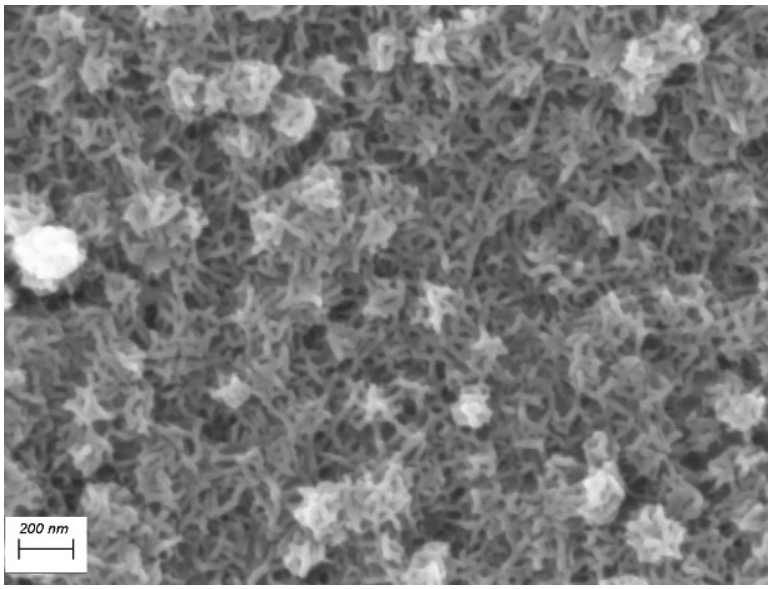

Figure S4. SEM images of the $Ni(OH)_2$ film electrodeposited for 5 minutes. (a) Overview of the surface morphology. (b) Magnified view revealing the nanofibrous structure.

The $Ni(OH)_2$ nanoparticles are uniformly distributed across the electrode surface despite the observation of some aggregates. The formation of these aggregates is likely due to high local current density and would be intensified under elevated temperature[4] and higher pH conditions of the electrolyte. A magnified view (b) demonstrates a continuous, porous structure of the $Ni(OH)_2$ film composed of ultra-thin nanofibres with diameters less than 30 nm.

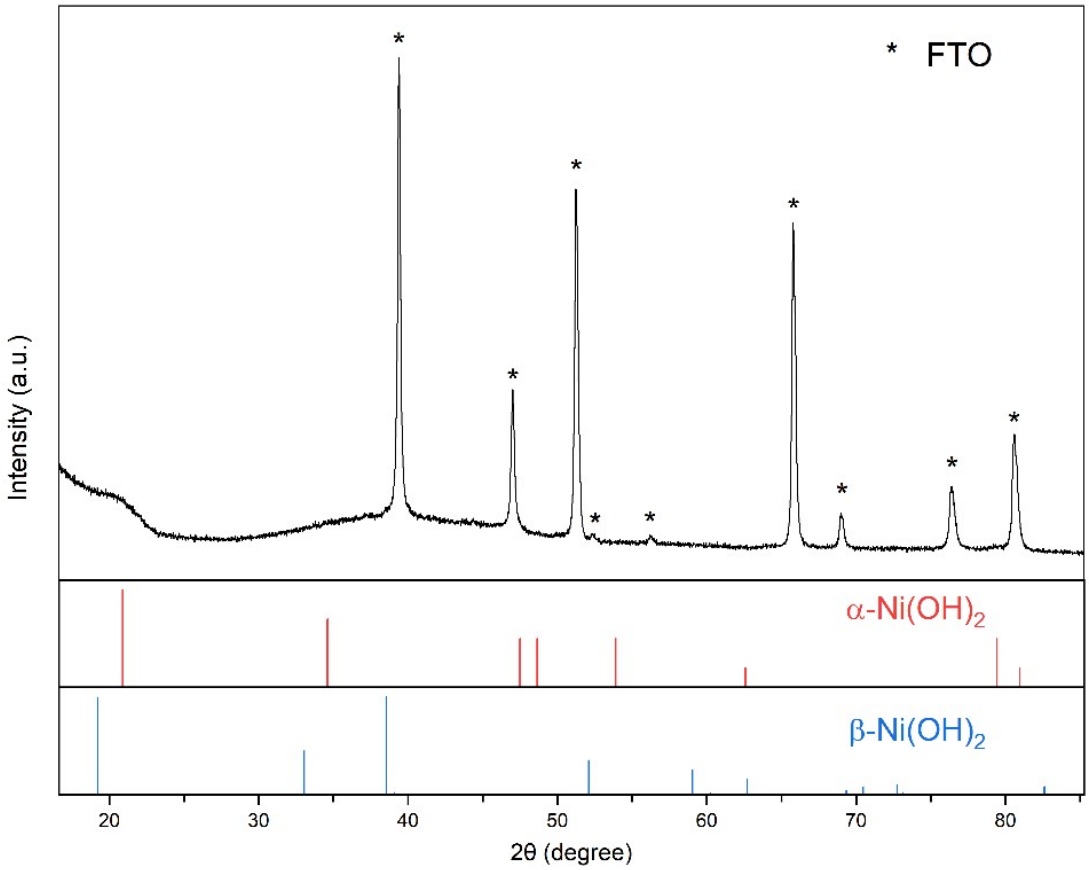

Figure S5. XRD pattern of the electrodeposited $Ni(OH)_2$ film on a FTO substrate.

Peaks labelled with asterisk (*) correspond to FTO, identified by the acquired XRD pattern of a pristine FTO substrate. No distinct diffraction peaks attributable to either α-$Ni(OH)_2$ (JCPDS 38-0715) or β-$Ni(OH)_2$ (JCPDS 14-0117) were observed, except for a broad hump around 10º, which shows resemblance to the (003) facet feature commonly associated with amorphous α-$Ni(OH)_2$.[5,6]

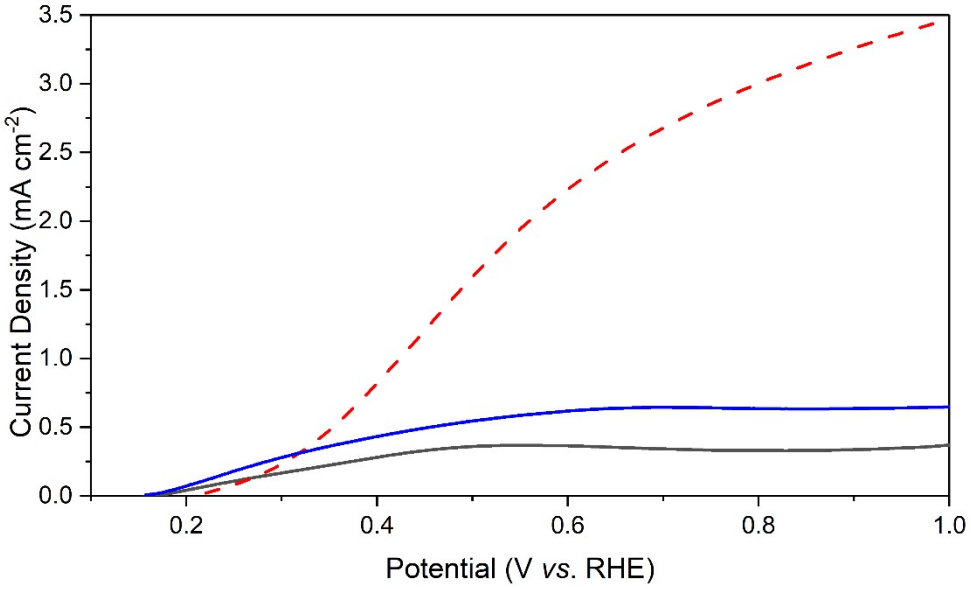

Figure S6. Photocurrent recorded using $Ni(OH)_2$-coated $BiVO_4$ photoanodes with (blue) and without (black) adding 1 M Na_2SO_3 as a hole scavenger in borate buffer (pH = 9.2). The red dashed line represents the LSV obtained using a pristine $BiVO_4$ electrode without $Ni(OH)_2$ coating. Scan rate = 10 mV s^{-1}

To investigate the direction of hole migration, LSVs were collected in the presence of 1 M Na_2SO_3 as a rapid hole scavenger. Compared with borate buffer alone (black line), the addition of Na_2SO_3 (blue line) led to a clear increase in photocurrent, confirming that a fraction of photogenerated holes is lost to recombination at the $BiVO_4$-$Ni(OH)_2$ interface due to the inefficient kinetics. At lower applied potentials the rate of recombination is relatively minor, and becomes increasingly pronounced with increasing potentials as $Ni(OH)_2$ depletes through oxidation to NiOOH. These results confirm that $Ni(OH)_2$ acts as a hole-accepting layer.

The photocurrent of bare $BiVO_4$ in the presence of 1 M Na_2SO_3 (red dashed line) was substantially higher than that of $Ni(OH)_2$-coated electrode. This indicates that forming a $BiVO_4$-$Ni(OH)_2$ (or -NiOOH) junction would intensify the interfacial recombination as a result of unfavourable band alignment.[7] The large photocurrent difference also indicates that direct contact between $BiVO_4$ and the electrolyte is minimised by the conformal $Ni(OH)_2$ coating, which likely suppresses competing reactions such as O_2 evolution occurring directly on the $BiVO_4$ surface.

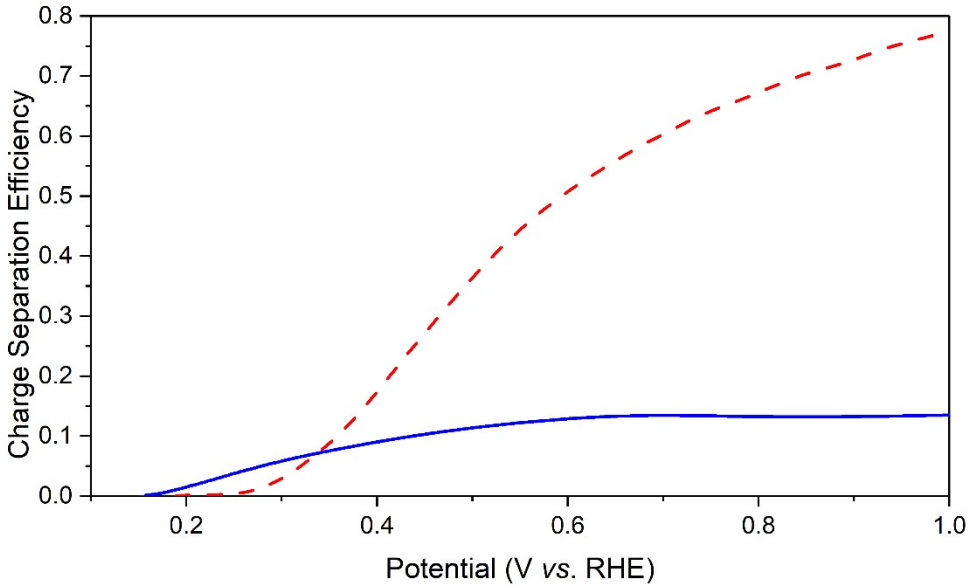

Figure S7. Charge separation efficiencies as a function of applied potential for the pristine $BiVO_4$ electrode (red, dashed) and the $Ni(OH)_2$-coated $BiVO_4$ electrode (blue).

The charge separation efficiency (η_{sep}) is one of the three factors governing external quantum efficiency for a PEC system, usually referred to as the incident photon-to-current efficiency (IPCE), together with the interfacial charge transfer efficiency (η_{int}) at the electrode-electrolyte interface and the charge generation efficiency (η_{gen}), as expressed in Eqn. S2.

$$IPCE_\lambda = \eta_{sep} \times \eta_{int} \times \eta_{gen} \#S2$$

η_{gen} represents the fraction of incident photons absorbed by the semiconductor and is equivalent to the light-harvesting efficiency (LHE) obtained from the UV-vis absorption spectra. In this study, the oxidation of SO^{2+}_3, a hole scavenger with fast oxidation kinetics, was employed. Under such conditions, the interfacial charge transfer is assumed to be kinetically facile ($\eta_{int} \approx 1$), and the interfacial charger recombination can be neglected. As a result, the measured photocurrent reflects the efficiency of charge separation within the semiconductor bulk. Therefore, the η_{sep} can be expressed as the internal quantum efficiency, also known as the absorbed photo-to-current efficiency (APCE) at a specific wavelength, as described in Eqn. S3.

$$\eta_{sep} = APCE_\lambda = \frac{IPCE_\lambda}{LHE_\lambda} = \frac{J_{ph}}{J_{abs}} \#S3$$

where J_{ph} is the measured photocurrent density and J_{abs} is the theoretical photocurrent assuming 100% separation of the photogenerated charge from the absorbed photons. To determine J_{abs}, the wavelength-dependent spectral intensity of the simulated sunlight was first converted into photon flux. The photon flux was then integrated over the wavelength range corresponding to photon energies above the bandgap of the photoelectrode, after being weighted by the LHE. The integrated photo flux was finally converted into the theoretical current density according to Eqn. S4.

$$J_{abs} = e \int \frac{P_\lambda \lambda}{hc} LHE_\lambda \, d\lambda \#S4$$

where e is the elementary charge, P_λ is the spectral intensity at wavelength λ, h is the Planck's constant, and c is the speed of light. The J_{abs} values calculated for a pristine $BiVO_4$ photoelectrode and for a $Ni(OH)_2$-coated $BiVO_4$ photoelectrode are 4.46 and 4.80 mA cm^{-2}, respectively.

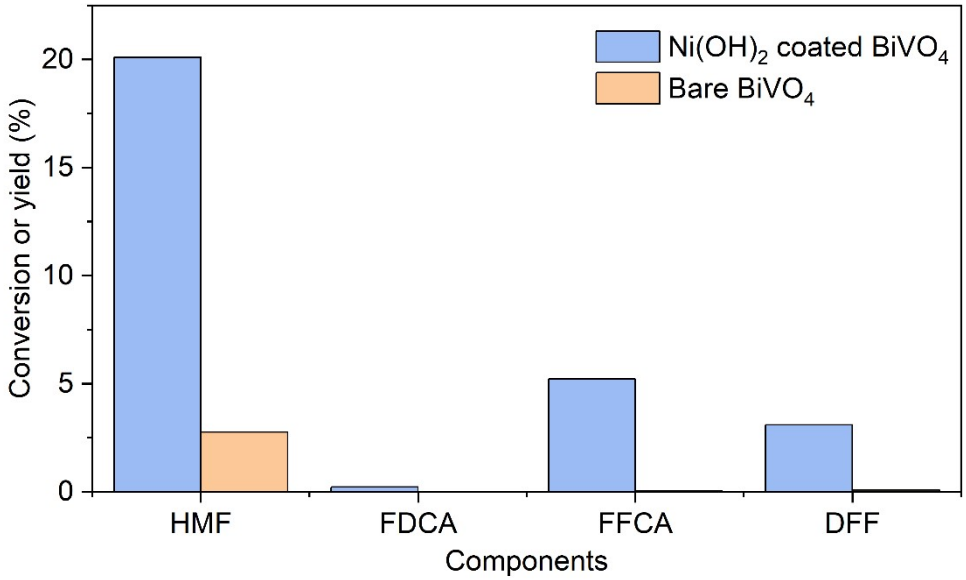

Figure S8. Comparison of HMF conversion and the oxidation product yields after 48 hours of PEC operation using $Ni(OH)_2$-coated $BiVO_4$ (blue) and pristine $BiVO_4$ (orange) photoanodes.

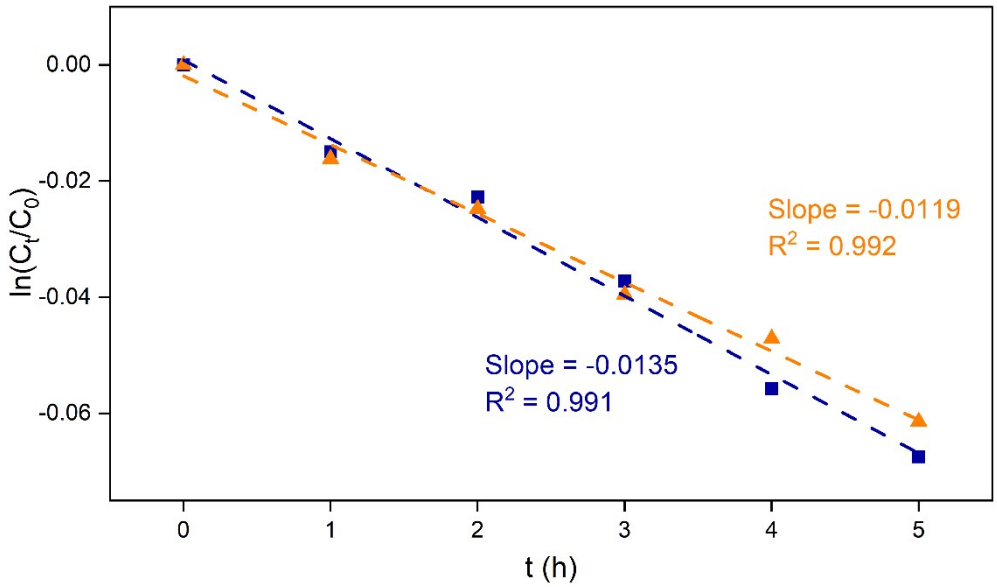

Figure S9. Kinetic analysis of HMF oxidation with $Ni(OH)_2$-coated $BiVO_4$ photoanode under PEC operation, represented by $\ln(C_t/C_0)$ *vs.* t for $C_{0,HMF}$ = 5 mM (blue) and 10 mM (orange) respectively. Linear fitted trendlines and the coefficients of determination R^2 are included in the plot.

The first 5 hours of the PEC operations were analysed as the subsequent accumulation of intermediates can competitively adsorb on the electrode surface, making the assumption that HMF oxidation dominates the electrode kinetics no longer valid.

The approximately linear trends obtained indicate that HMF oxidation by the locally generated NiOOH followed first-order kinetics at both 5 mM and 10 mM initial concentrations, with only minor variation in the fitted gradients (-k). Although it should be acknowledged that the limited conversion of HMF within the studied range prevent a definitive statement with absolute certainty, the results support the validity of a pseudo-first-order description.

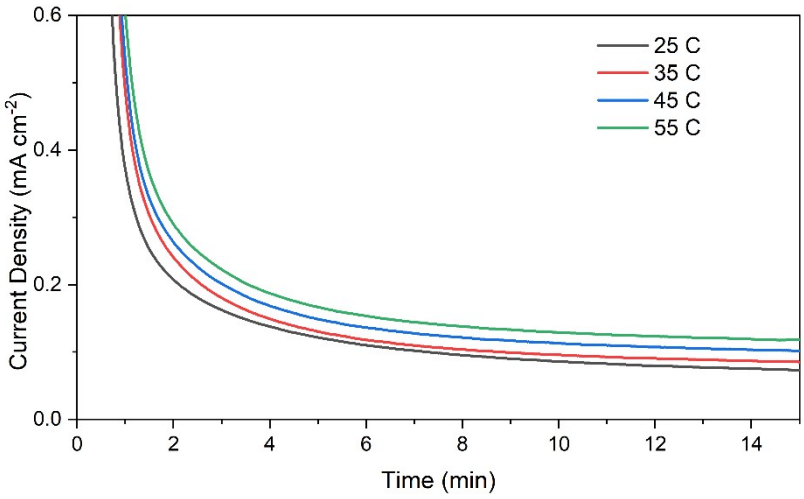

Figure S10. Photocurrent densities recorded over 15 minutes from the start at 1.05 V *vs.* RHE under constant illumination (AM 1.5 G, 100 mW cm^{-2}) with 5 mM HMF in borate buffer.

Electrolyte temperature was varied from 25 to 55 ºC while other conditions were kept constant. The electrolyte was circulated through the laminar flow cell chamber at 5 mL min^{-1}.Varying the flow rate showed no significant effect on current densities. Average current densities were calculated from the final 20 data points (recorded over 2 seconds) of each measurement after establishing steady-state operation.

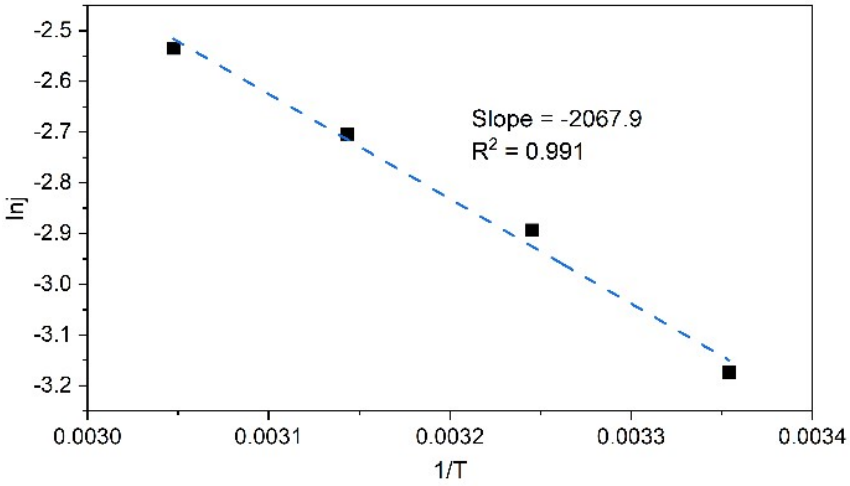

Figure S11. Arrhenius plot derived from the PEC measurements under various temperature conditions range from 25 to 55 ºC.

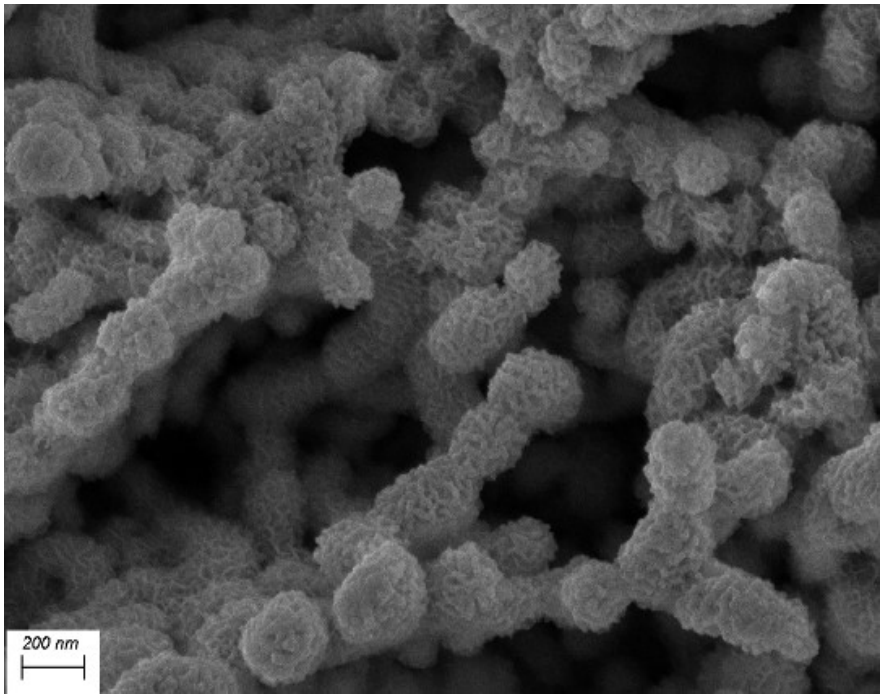

Figure S12. Post-reaction SEM characterisation of the $Ni(OH)_2$-decorated $BiVO_4$ photoanode recovered after a 48-hour reaction.

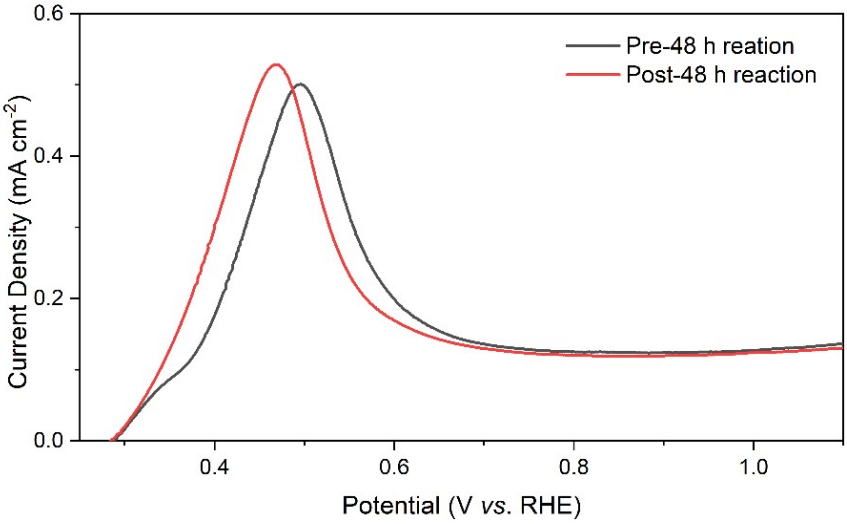

Figure S13. Comparison of LSV scans measured in freshly prepared electrolyte containing 5 mM HMF, using the photoanode before (black) and after (red) and 48-hour PEC operation. Scan rate = 10 mV s^{-1}.

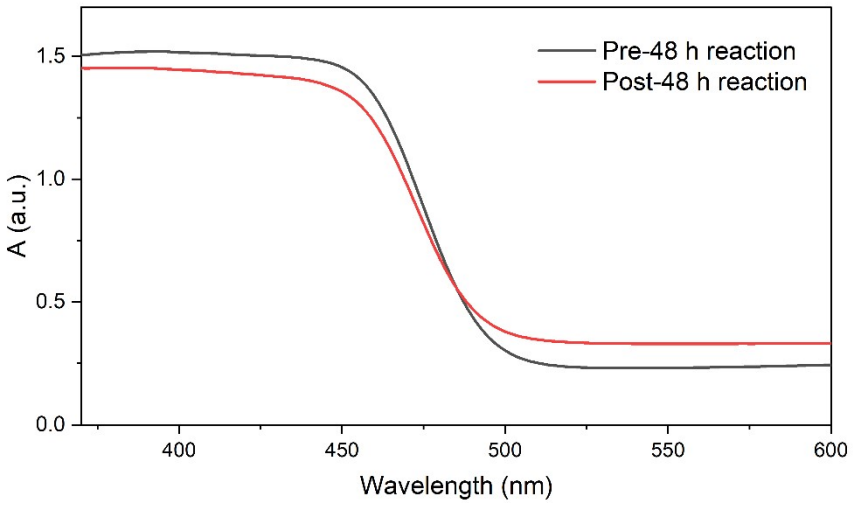

Figure S14. UV-vis absorbance spectra of the $Ni(OH)_2$-coated $BiVO_4$ photoanode collected before and after a 48-hour PEC operation performed in a strongly alkaline electrolyte (pH = 13). Five CV cycles were before prior to each measurement to minimise the NiOOH residue.

To further evaluate the electrode stability and its robustness under strongly alkaline conditions, the PEC operation was repeated in borate buffer with adjusted to pH = 13 by the addition of NaOH, while maintaining all other experimental conditions. A clear enhancement in photocurrent was observed at the initial stage, which can be attributed to multiple factors, including the increased ionic conductivity of the electrolyte, accelerated OER kinetics arising from the higher OH^- concentration, and the possibly enhanced rate of HMF oxidation at elevated pH, as often reported in the literature.[1] However, photocurrent continuously decayed throughout the 48-hour operation, in contrast to the near-stabilised response typically achieved after 5 to 6 hours of operation under pH = 9.2 conditions.

Product analysis revealed an increase in HMF conversion from 20.1% on average for pH = 9.2 cases to 46.6%, accompanied by only marginal increase in FDCA yield, from 0.23% to 0.27%. This observation suggests that the higher conversion of HMF cannot be solely attributed to the improved reaction kinetics but rather to the dominance of alkaline-promoted HMF degradation. Compared to near-neutral conditions, HMF is significantly more prone to side reactions such as hydration and polymerisation, leading to the formation of humins and other undetectable by-products, as widely reported in previous studies.[1,8,9] Such degradation has been reported to be intensified with elevated temperature, which was also inevitable in the present study due to the photons absorbed by the electrolyte.[8]

The UV-vis absorbance spectra collected before and after the 48-hour reaction showed a notable decrease in absorption across the $BiVO_4$ photoactive region ($\lambda < 480$ nm), indicating partial etching or deactivation of the photoelectrode under concentrated alkaline conditions. This occurred despite the presence of $Ni(OH)_2$ overlayer, which minimised direct contact between $BiVO_4$ and the electrolyte. In contrast, a moderate increase in absorbance was observed at longer wavelengths ($\lambda > 480$ nm). Although the exact contributions for this feature cannot be conclusively determined in this work, several plausible factors, including the

deposition of the polymeric by-products formed during the reaction, and, more likely, the presence of NiOOH residue that persisted on the photoelectrode surface despite the CV pretreatment prior to measurement.

References:

1 L. Gálvez-Vázquez, A. Dutta, S. Vesztergom, Z. Szakály, R. Zaugg, A. V. Rudnev and P. Broekmann, *J Catal*, DOI:10.1016/j.jcat.2025.116321.

2 M. Kim, Y. Su, A. Fukuoka, E. J. M. Hensen and K. Nakajima, *Angewandte Chemie*, 2018, **130**, 8367–8371.

3 J. C. Velasco Calderón, J. S. Arora and S. H. Mushrif, *ACS Omega*, 2022, **7**, 44786–44795.

4 Y. M. Wang, D. D. Zhao, Y. Q. Zhao, C. L. Xu and H. L. Li, *RSC Adv*, 2012, **2**, 1074–1082.

5 D. S. Hall, D. J. Lockwood, C. Bock and B. R. MacDougall, *Proceedings of the Royal Society A: Mathematical, Physical and Engineering Sciences*, 2015, **471**, 20140792.

6 M. Aghazadeh, M. Ghaemi, B. Sabour and S. Dalvand, *Journal of Solid State Electrochemistry*, 2014, **18**, 1569–1584.

7 T. W. Kim and K. S. Choi, *Science (1979)*, 2014, **343**, 990–994.

8 P. Díaz-Maizkurrena, J. Requies, A. Iriondo and M. Macías-Villasevil, *Catal Today*, DOI:10.1016/j.cattod.2025.115338.

9 M. L. Krebs, A. Bodach, C. Wang and F. Schüth, *Green Chemistry*, 2023, **25**, 1797–1802.